Published in final edited form as:
NMR Biomed. 2011 December ; 24(10): 1313–1325. doi:10.1002/nbm.1693.

Measurement of Absolute Arterial Cerebral Blood Volume in Human Brain Without Using a Contrast Agent

Jun Hua[1,2], **Qin Qin**[1,2], **James J. Pekar**[1,2], and **Peter C. M. van Zijl**[1,2,*]

[1] The Russell H. Morgan Department of Radiology and Radiological Science, Division of MR Research, The Johns Hopkins University School of Medicine, Baltimore, MD USA

[2] F.M. Kirby Center for Functional Brain Imaging, Kennedy Krieger Institute, Baltimore, MD USA

Abstract

Arterial cerebral blood volume (CBV_a) is a vital indicator of tissue perfusion and vascular reactivity. We extended the recently developed inflow vascular-space-occupancy (iVASO) MRI technique, which uses spatially selective inversion to suppress the signal from blood flowing into a slice, with a control scan to measure absolute CBV_a using CSF for signal normalization. Images were acquired at multiple blood nulling times to account for the heterogeneity of arterial transit times across the brain, from which both CBV_a and arterial transit times were quantified. Arteriolar CBV_a was determined separately by incorporating velocity-dependent bipolar crusher gradients. Gray matter CBV_a values (n = 11) were 2.04 ± 0.27 and 0.76 ± 0.17 ml blood/100 ml tissue without and with crusher gradients (b = 1.8 s/mm^2), respectively. Arterial transit times were 671 ± 43 and 785 ± 69 ms, respectively. The arterial origin of the signal was validated by measuring its T_2, which was within arterial range. The proposed approach does not require exogenous contrast agent administration, and provides a noninvasive alternative to existing blood volume techniques for mapping absolute CBV_a in studies of brain physiology and neurovascular diseases.

Keywords

cerebral blood volume; arterial blood volume; arterial transit time; double inversion; iVASO; VASO; perfusion; MRI

Introduction

Arterial cerebral blood volume is an important indicator of tissue function and viability. Arterial vessels, here defined as the combination of arteries, pial arteries and arterioles, are the driving source to supply the tissue with oxygen and other nutrients (1). The local tissue perfusion is primarily regulated through vasodilatation or constriction of the smaller pial arteries and arterioles with diameters up to 100–150 microns (1–3). Therefore, the ability to determine the volume of these arterial microvessels (CBV_a) separately from other vascular compartments (capillary and venous) provides information that is not obtainable from total cerebral blood volume (CBV_{tot}). Defining parenchymal microvessels as those with diameters of up to 200 microns, CBV_{tot} is about 5.5% in gray matter (GM) and 1.5% in white matter (WM) (4), while CBV_a constitutes about 20% of CBV_{tot} (5). Measurement of CBV_a *in vivo* requires some type of selective labeling of arterial blood. This is complicated, but several promising approaches have recently been published. First, using the fact that

Corresponding Author: Jun Hua or Peter C.M. van Zijl, Johns Hopkins University School of Medicine, Dept. of Radiology, 217 Traylor Bldg, 720 Rutland Ave, Baltimore, MD, 21205, jhua@mri.jhu.edu or pvanzijl@jhu.edu, Tel: 443-923-9500, Fax: 443-923-9505.

blood velocity is higher in arterial vessels than post-arterial vessels, magnetic field gradients (6,7) can be employed to predominantly dephase the signal from the arterial compartment, allowing estimation of CBV_a by comparing images with and without such crusher gradients (8–11). However, as the blood flow in both arteries and arterioles may be affected by the crusher gradients, it is not trivial to separate macro- and micro-vascular components by using this method alone. A second approach to separate arterial and post-arterial blood is based on oxygenation level and employs the magnetic field variation induced by paramagnetic deoxyhemoglobin (12–14). Such methods are sensitive to background macroscopic field inhomogeneity, but this can be corrected for by performing an extra field map scan (13). A third approach is to exploit the impermeability of the arterial vessels by administrating diffusible exogenous contrast agents (15,16) or adopting the blood water protons as endogenous tracers (16–19) using the arterial spin labeling (ASL) methodology. By modulating the tissue signal using techniques such as magnetization transfer (MT) (16), selective saturation (19) or progressive saturation (17,18), CBV_a information can be extracted.

Here, we demonstrate a new approach of the third category to measure absolute CBV_a in physiological units based on the vascular-space-occupancy (VASO) MRI (20–22) approach, in which blood signal is removed by inverting its magnetization and acquiring images when it crosses zero during T_1 recovery. In a recent extension to the conventional VASO approach, dubbed inflow VASO (iVASO) (23,24), we showed that arterial selective blood nulling can be achieved by employing spatially selective inversion so that only the blood flowing into the slice is nulled. We show here that iVASO can be used to selectively quantify the signal from the arterial compartment on a voxel-by-voxel basis through comparison with a control scan without blood nulling and by measuring at a series of repetition time (TR) dependent blood nulling times to account for the heterogeneity of arterial transit times in the cortex. Furthermore, by incorporating crusher gradients in *both* nulling and control scans, the signal can be sensitized predominantly to arteriolar CBV_a. Part of this work has been reported in abstract form (25).

At the same time this paper was being prepared, another article (26) appeared proposing a similar approach. Both methods, based on the iVASO approach originated by Hua et al. (23,24), were independently conceived and previously reported simultaneously in abstract form (25,27). While the work by Donahue et al. (26,27) is mainly intended to test the clinical feasibility in stroke patients, the current paper focuses on technical development of the approach in normal subjects, which differs from the former in that: 1) a theoretical framework is developed to account for arterial transit times and tissue perfusion; 2) multi-TI experiments are carried out from which both CBV_a and transit times are measured; 3) large vessel contributions are removed experimentally using crusher gradients; and 4) the arterial origin of the signal is proven using relaxation time measurements.

Materials and Methods

ASL and VASO

The difference between arterial spin labeling (ASL) (28,29) and VASO (20) contrast is sometimes confusing. Actually, with respect to the pulse sequences, VASO and iVASO scans are the same as the spatially non-selective and selective inversion components of pulsed ASL, respectively. In VASO and iVASO, images are acquired at one specific inversion time (TI), at which blood signal is nulled (labeled), which provides signals proportional to CBV_{tot} and CBV_a changes, respectively. In iVASO, the impermeable arterial compartment is highlighted by nulling arterial blood while keeping full signal in other compartments, whereas ASL exploits the exchange between capillary blood and tissue to measure tissue perfusion or cerebral blood flow (CBF) (Fig. 1), which has to use a TI longer

than for blood nulling to eliminate the unwanted arterial blood effects and maximize the water exchange effects in the capillary bed (7,30–32).

Pulse sequence

Fig. 2 illustrates the timing and inversion scheme of the iVASO pulse sequence for determining absolute CBV_a, which consists of two consecutive scans: blood nulling and control. In the spatially-selective nulling scan, a non-selective adiabatic inversion pulse is followed immediately by a spatially selective inversion pulse to flip back the water spins in the imaging slice and the brain superior to it, so that the effect from potential inflowing venous blood is minimized. This nulling scan is identical to Sequence IIb proposed in the original iVASO paper (23,24). Images are then acquired at the time when the inverted blood water spins that flow into the slice are nulled. To be able to determine the amount of blood nulled in the slice, the signal needs to be compared with a control scan (Fig. 2, bottom) performed with two consecutive spatially non-selective inversion pulses and identical imaging parameters. Importantly, for the flip back pulse in the control scan, its bandwidth and frequency offset relative to the resonance frequency of spins in the imaging slice should be identical to those in the nulling scan, such that any off-resonance MT effects for the spins in the slice are identical in both scans. In an effort to keep the effect of potential eddy currents comparable for the nulling and control scans, the spatial selection gradient for the flip back pulse is also included in the control scan, but shifted to not coincide with the RF pulse.

Fig. 3a illustrates the evolution of the longitudinal magnetizations from static tissue (blue), blood in the imaging slice (green) and inflowing blood before reaching the slice (red), for a series of interleaved nulling and control scans (TR/TI = 2.5/0.81 s) using numerical Bloch equation simulations (T_1 of blood/tissue taken as 1.627/1.15 s (33,34), respectively). Signal of the inflowing blood will switch from the red curve to the green curve after the blood enters the imaging slice. A spatially non-selective saturation (90° RF pulse followed by dephasing gradients, shown in Fig. 2) is applied immediately after each imaging module to set all magnetizations (blood and tissue) to zero. The purpose of this pulse is two-fold. One is to establish a steady state of blood signal after the first nulling scan regardless of what TR used (35,36), which is particularly important when imaging brain regions with fast blood flow velocity or when using a small transmission coil that has limited coverage of the feeding arteries. The second purpose of the saturation pulse is to make sure that only blood entering during period 1 (marked in Fig. 3a) will be nulled at TI in the nulling scan, while blood entering during other periods will be at its steady state full signal at TI in the nulling and control scans. This guarantees only blood flowing in during TI in the nulling scan will contribute to the difference signal. Without this post-acquisition saturation pulse, blood entering during period 3 (Fig. 3a) would be more relaxed than its steady state full signal at TI in the following nulling scan, because the spins would no longer be inverted (instead, flipped back) after entering the imaging slice, which would result in an underestimation of blood volume.

Theory

The steady state blood nulling time (TI) can be determined from (20,23):

$$1 - 2 \cdot e^{-TI/T_1} + e^{-TR/T_1} = 0, \quad [1]$$

Note that because of the magnetization reset effect from the post-acquisition saturation pulse, the steady state blood nulling time is still calculated from one TR, instead of two times TR, despite the interleaving of nulling and control scans. At 3 Tesla (3T), the blood

nulling times range from approximately 200 ms to 1100 ms for TR = 500–7000 ms (21), which approximates the arterial transit times reported for human brain GM (400–1400 ms, (18,37–40)). As a consequence, iVASO is expected to achieve predominantly arterial selective blood nulling. Using the iVASO theory developed in Hua et al. (23,24), the steady state difference signal (S_{diff}) between the nulling and control scans for a gradient echo (GE) imaging sequence can be derived to be (details in Appendix):

$$S_{diff}=S_{ctrl}-S_{null}$$

$$\begin{cases} =0, & \text{when } TI<\Delta \\ =M_0\cdot C_b\cdot(CBV_a/\delta_a)\cdot(TI-\Delta)\cdot(1-e^{-TR/T_{1,a}})\cdot e^{-TE/T^*_{2,a}}, & \text{when } \Delta\le TI\le\Delta+\delta \\ =M_0\cdot[C_b\cdot CBV_a\cdot(1-e^{-TR/T_{1,a}})\cdot e^{-TE/T^*_{2,a}} \\ \quad +C_b\cdot(1-E)\cdot f\cdot TI_{ex}\cdot e^{TI_{ex}\cdot(1/T_{1,a}-1/T_{1,c})}(1-e^{-TR/T_{1,a}})\cdot e^{-TE/T^*_{2,c}} & \text{when } \Delta+\delta_a<TI\le\Delta \\ \quad +C_t\cdot\left(\frac{E\cdot f}{\lambda}/\left(\frac{1}{T_{1,app}}-\frac{1}{T_{1,c}}\right)\right)\cdot\left(e^{-TI_{ex}/T_{1,c}}-e^{-TI_{ex}/T_{1,app}}\right)\cdot e^{-TI_{ex}/T_{1,a}}\cdot\left(1-e^{-TR/T_{1,a}}\right)\cdot e^{-TE/T^*_{2,t}}], & \end{cases}$$

[2a]

in which

$$\frac{1}{T_{1,app}}=\frac{1}{T_{1,t}}+\frac{E\cdot f}{\lambda} \quad [2b]$$

$$TI_{ex}=TI-\Delta-\delta_a \quad [2c]$$

The parameters in Eq. [2] are defined in Table 1 and values from the literature are provided. Notice that f represents CBF in units of ml/ml/s (compared with conventional units of ml/100 ml/min). Three situations are considered in Eq. [2]. For $TI<\Delta$, no inverted blood water has reached the imaging slice, and nulling and control signals are identical. For $\Delta \le TI \le \Delta + \delta_a$, inverted blood has flowed into the slice but has not passed through the arterial compartment. In view of the impermeability of arterial vessels, negligible exchange between blood and tissue water is assumed during this period. Thus the difference signal simply reflects the amount of inflowing blood. For $\Delta + \delta_a < TI \le \Delta + \delta_a + \delta_c$, the inverted blood has reached the capillary bed, and the difference signal has three contributions (Appendix): 1) the entire arterial compartment that is filled with inverted blood water protons; 2) inflowing blood water protons that remain in the capillaries (fraction = 1-E) and still follow the VASO principle (inversion recovery); 3) inverted blood water protons that exchange with tissue water protons (fraction = E). At 3T, the longest blood nulling time (about 1100 ms) is not enough for blood to traverse the entire capillary network ($\Delta + \delta_a + \delta_c \approx$ 1.5–2 s, Table 1). Therefore TI values longer than $\Delta + \delta_a + \delta_c$ are not considered.

The fraction E, defined by Silva et al (41) as the "extraction fraction" for water, is generally a function of blood flow and ranges from 0 to 1. In Fig. 3b, the difference signal is simulated as a function of TI assuming complete exchange (E = 1, red) or no exchange (E = 0, green) in the capillary compartment. The largest difference between the red and green curves is 2–3% of S_{diff}, or 0.02–0.03% of total signal (S_{ctrl} or S_{null}) and negligible within experimental

error. Furthermore, it is assumed in Eq. [2] that exchange takes place instantaneously, i.e. as soon as the inverted blood enters the capillaries. However, the average water exchange time in the capillary compartment has been reported to be 0.5–1 s (42,43), which will make the actual influence even smaller. We therefore assume E = 0.5 (41) for all following calculations. One potentially confounding factor for $\Delta + \delta_a < TI \leq \Delta + \delta_a + \delta_c$ is that inflowing blood that remains in the capillaries (the second term) would no longer be nulled exactly at TI, if T_1 of capillary blood is very different from that of arterial blood. However, in view of only a small difference between measured T_1 of arterial (1664 ms) and venous (1584 ms) blood at 3T (33), and the small fraction of capillary blood contributing to the total iVASO effect, it is safe to assume a similar blood T_1 for all vascular compartments (Table 1). Eq. [2] can thus be simplified with the above two assumptions. At higher magnetic fields, however, these assumptions may need to be re-evaluated.

If the transit times (Δ, δ_a) would be known, the difference image could be used as a relative CBV_a map, and CBV_a could be quantified using Eq. [2] from a single scan for $\Delta \leq TI \leq \Delta + \delta_a$. Unfortunately, the transit times are not uniform across cortical regions and generally not precisely known. To account for transit time heterogeneity, images can be acquired at multiple TIs, from which three or four unknowns (CBV_a, Δ, δ_a, and f, depending on the length of transit) can be fitted with Eq. [2] on a voxel-by-voxel basis.

M_0, which is a constant giving the MR signal per unit volume of water protons at equilibrium, can be estimated from a pure cerebrospinal fluid (CSF) voxel using a reference scan without inversion (4), or from a nulling or control scan using the following equation:

$$S_{CSF} = M_0 \cdot C_{CSF} \cdot \left(1 - e^{-TR/T_{1,CSF}}\right) \cdot e^{-TE/T^*_{2,CSF}} \quad [3]$$

in which C_{CSF} = 1 ml water/ml CSF, $T_{1,CSF} \approx 3817$ ms (34) and $T_2^*{}_{,CSF} \approx 1442$ ms. When long TR and short TE are used for the reference scan, the CSF signal will be at full relaxation so that Eq. [3] can be simplified to $S_{CSF} = M_0$ (4). Notice that the definition of M_0 varies in literature. In some instances, M_0 contains the effect of water density (C_b), and in others, M_0 and C_b are two separate parameters in the equation. In our model, the latter convention is used and $M_0 * C_b$ represents the equilibrium MR signal in the blood.

MRI Experiments

Experiments were conducted on a 3T human MRI scanner (Philips Medical Systems, Best, The Netherlands). A body coil (approximately 650 mm in axial length) was used for RF transmission and a 32-channel phased-array head coil (In Vivo, Corporation, Florida) was used for reception. Pulse sequences were verified on a phantom containing 18% cross-linked bovine serum albumin (BSA) phantom, after which measurements were performed on 11 healthy subjects (5 male and 6 female) who gave written informed consent before participating in this Johns Hopkins Institutional Review Board (IRB) approved, Health Insurance Portability and Accountability Act (HIPAA)-compliant study. All subjects participated in Experiment I (see below) whereas 5 subjects took part in Experiment II. For all subjects, the imaging slice was carefully placed at approximately the same location of the cortex: about 2 mm superior to the corpus callosum and angled through the posterior lobe, as illustrated in Fig. 2. The flip back slab was 80 mm and its bottom edge was 7 mm inferior to the bottom of the imaging slice.

Experiment I: Eight different combinations of TR/TI were used: TR/TI = 5000/1054, 3100/902, 2500/811, 2000/711, 1667/629, 1300/523, 1000/424 and 650/293 ms, with which interleaved nulling and control scans were repeated 10/15/15/18/18/30/40/70 times,

respectively, which took 1′40″/1′33″/1′15″/1′12″/1′01″/1′18″/1′20″/1′18″, respectively. The number of repetitions for each TR was determined to achieve comparable signal-to-noise ratio (SNR) in GM for all TRs. A single-shot gradient-echo echo-planar-imaging (GE-EPI) readout was employed with fat suppression to reduce fat shift artifacts. Volume shimming (first order) was used to ensure homogeneity in the entire brain, which is important for proper inversion over the complete volume. Other imaging parameters: TE = 22 ms, flip angle = 90°, voxel = 3 mm isotropic, matrix = 96×96, single-slice, SENSE factor = 2.5. Bipolar crusher gradients were applied in both nulling and control scans to selectively dephase the signal from the fast flowing water protons in arteries, thereby sensitizing iVASO predominantly to arteriolar CBV. To assess their effects, three crusher gradient strengths (b = 0, 0.3, 1.8 s/mm^2, corresponding to velocity encoding (V_{enc}) of infinite, 10, 3 cm/s, respectively) were applied in the z-direction. Four sets of iVASO scans (each with eight TR/TI combinations) were performed on each subject, with three sets using different crusher gradients and the fourth set increasing the gap between imaging slice and inversion slab from 7 to 17 mm (b = 1.8 s/mm^2). The order of the four sets and of the scans within each set was pseudo-randomized to avoid potential bias from systemic physiological variations over time. To determine M_0, a long TR and short TE reference scan (without inversion) through the ventricle was obtained (TR/TE = 20 s/13 ms, other imaging parameters the same, 3 repetitions, scan duration = 1′). The constant level appearance (CLEAR) algorithm (Philips Medical Systems, Best, The Netherlands), which calculates the proper signal contribution of each voxel based on a coil sensitivity map from a reference scan, was applied for receive inhomogeneity correction. A whole-brain 3D magnetization prepared rapid acquisition gradient echo (MPRAGE) scan (TR/TE/TI = 8.3/3.8/832 ms, voxel = 1 mm isotropic, 151 slices, middle of the volume aligned with the single slice iVASO scans) was performed for anatomical reference. All images for each subject were acquired using identical gain settings on the scanner.

Experiment II: To validate the arterial origin of the difference signal (S_{diff}), its transverse relaxation time (T_2), which is highly oxygenation level dependent (44–48), was measured with a Carr-Purcell-Meiboom-Gill (CPMG) (49–53) based pulse sequence (n = 5). T_2 preparation modules (52,53) with 0/2/4/8/16 refocusing pulses (inter-echo spacing = 10 ms) corresponding to effective TEs (TE_{eff}) of 0/20/40/80/160 ms, were added before the excitation pulse in both nulling and control scans (Fig. 2). Note that it is important to use spatially non-selective pulses in the T_2 preparation module, which helps to minimize the well-known blood outflow effect (54). For each TE_{eff}, six iVASO scans with TR/TIs of 5000/1054, 3100/902, 2500/811, 2000/711, 1667/629 and 1300/523 ms were performed with the same respective repetitions as in Experiment I. The gap between imaging slice and inversion slab was kept at 7 mm and crusher gradients of b = 1.8 s/mm^2 were applied. Notice that we chose to measure T_2 instead of T_2* of the iVASO signal because 1) the difference between arterial and capillary (77% oxygenation based on the assumption of exponential oxygenation decay in the capillaries, details in Table 1) blood T_2 values is larger (at 3T, T_2 = 138 v.s. 96.6 ms (48), T_2* = 54.9 v.s. 30.5 ms, Table 1), and 2) the spatially selective RF pulses used in multi-echo GE T_2* measurements may cause contamination from the blood outflow effect (54), especially for single slice acquisition.

Data Analysis

Images were motion-corrected using the Automated Image Registration (AIR) algorithm (55). The first pair of nulling and control images acquired for each TR/TI were not included when averaging, as they may not have reached steady state. The surround subtraction method, in which the nulling/control images are subtracted by the linear interpolation between the surrounding control/nulling images (56), was employed to calculate S_{diff}, after which the S_{diff} images for each TR/TI were averaged. In Experiment I, the maps of CBV_a, Δ,

δ_a, f were then numerically fitted with Eq. [2] and the multi-TI S_{diff} data. In Experiment II, the apparent T_2 for the inflowing blood was mono-exponentially fitted from the five TE_{eff} data. GM and WM masks for each subject were generated using the MPRAGE images and the Medical Image Processing, Analysis, and Visualization (MIPAV) application (http://mipav.cit.nih.gov/). The standard deviation of a difference map from two consecutive images (after steady state is reached) was used to estimate the noise level (N) and calculate SNR, which is defined as $(S/N)\cdot\sqrt{NSA}$ (NSA=number of signals averaged). A threshold of one standard deviation (SD) below the mean SNR was used to exclude voxels with insufficient SNR from GM and WM masks. Only voxels that had sufficient SNR at all TIs were included when averaging. All programs were coded in Matlab 6.0 (Mathworks, Natick, MA, USA).

Results

First, the ability of the pulse sequence to remove static signal was verified on a phantom (18% cross-linked BSA) with a T_1 and T_2 comparable to normal brain tissues and a strong MT effect. The difference signals for TR values of 5 s and 2 s were 0.03±0.26% and −0.05±0.27% of the original control signal, respectively, which is within the noise level and not significantly different from zero ($P > 0.1$). This demonstrates that potential contaminations such as off resonance MT effects and incomplete inversion are expected to be minimal.

Fig. 4 and Table 2 show representative results for one subject (gap = 7 mm, b = 0.3 s/mm^2). Comparable data were consistently observed in all subjects. The effect of inflowing blood in the S_{diff} images can be clearly seen in Fig. 4a. Table 2 shows the GM SNR of nulling and control images, as well as the contrast-to-noise ratio (CNR) for the S_{diff} images obtained, all calculated on a voxel-by-voxel basis and then averaged over GM voxels. The SNR and CNR values are comparable ($P > 0.1$) among all TR/TIs. Fig. 4b displays the average S_{diff} in GM and WM for this subject as a function of TI. In GM, S_{diff} increases as inverted blood flows in, which can be fitted by the iVASO theory (Eq. [2]). The standard deviations (SD) for these GM S_{diff} values are quite large, which we tentatively attribute to heterogeneity of CBV_a and arterial transit times over different cortical regions. In WM, on the other hand, S_{diff} is not significantly elevated from zero ($P > 0.1$) with smaller SDs compared to GM. This is expected in view of the longer arterial transit times in WM (at least 1–2 s (57,58)), which are mostly outside the TI range for iVASO at this field strength. As MT effects in WM are about double those in GM, this result confirms that MT contamination is minimal. Fig. 4c shows the fitted maps of CBV_a, Δ, δ_a, f for this subject. The average values in GM for this subject were: CBV_a = 1.28 ± 0.80 ml/100 ml, Δ = 401 ± 124 ms, δ_a = 341± 158 ms, f = 63.6± 38.9 ml/100 ml/min ((1.06± 0.65) × 10^{-2} ml/ml/s). While the maps of CBV_a, Δ, δ_a showed reasonable contrast, the f map was not as reliable, indicating that the fitting is not quite sensitive to this parameter. This is not unexpected, as f becomes relevant only in the capillaries. Therefore, in subsequent calculations for all subjects, we performed fitting with Eq. [2] both for all four unknowns (CBV_a, Δ, δ_a, f, free fitting) and only three of them (CBV_a, Δ, δ_a) with an assumed CBF value of 55 ml/100 ml/min (0.92 × 10^{-2} ml/ml/s) (Table 1).

In Table 3, the average values (n = 11) of CBV_a, Δ, δ_a, f in GM are summarized. As expected, the use of a preset flow value gave comparable ($P > 0.1$) fitting results for all other three parameters. When increasing the crusher gradient strength, CBV_a reduces appreciably ($P < 0.01$), while the time needed for inverted blood to traverse the gap between inversion and image planes (Δ) prolongs ($P < 0.01$). The mean transit time for blood in the arterial compartment (δ_a) remained comparable ($P > 0.1$) for b = 0 and 0.3 s/mm^2, but increased for b = 1.8 s/mm^2. No significant difference ($P > 0.1$) was found in CBV_a, Δ, δ_a between scans

with different gaps (7 and 17 mm) between imaging slice and inversion slab. Note that although the intra-subject SDs were large (Fig. 4), the inter-subject SDs were much smaller.

To assess the influence from the assumed blood T_1 value (1627 ms) on the fitting results, we repeated the fitting procedure on the data sets (n = 11) with gap = 7 mm and crusher b value = 0.3 s/mm^2, assuming two different blood T_1 values: 1664 ms (92% oxygenation) and 1584 ms (69% oxygenation) (33), respectively. The fitted parameters in GM were: CBV_a = 1.28 ± 0.23 (blood T_1 = 1664 ms) and 1.25 ± 0.19 (blood T_1 = 1584 ms) ml/100 ml, Δ = 335 ± 25 and 351 ± 19 ms, δ_a = 367 ± 31 and 353 ± 27 ms, respectively. No statistical difference was found between these fitted results ($P > 0.1$), confirming our assumption that using a single blood T_1 for all intravascular compartments has negligible effect at 3T. Similarly, to evaluate the effect from the fixed CBF value, we repeated the fitting procedure on the same data sets assuming GM CBF values of 40 and 65 ml/100 ml/min, respectively (GM CBF value has been consistently reported in the range of 40–65 ml/100 ml/min (59,60)). Comparable results were obtained ($P > 0.1$), which again indicates that the fitting is not very sensitive to this parameter. Note that at 3T, the assumed CBF value should only affect the GM voxels, as the arterial transit time in WM is reportedly (57,58) outside the iVASO TI range so that the amount of inverted blood that can reach the capillary perfusion zone in WM at 3T is negligible.

Fig. 5 shows the T_2 values (n = 5, Experiment II) for S_{diff} averaged over GM regions as a function of TI (asterisk), which are in the range of 120–145 ms for TI < 1000 ms, comparable to arterial blood T_2 measured *ex vivo* using a similar CPMG sequence (τ_{CPMG} = 10 ms) (48). At TI = 1054 ms, the T_2 value for S_{diff} became lower ($P < 0.05$). Note that these difference signals reflect the inflowing blood over the entire span of TI. We also calculated T_2 for the inflowing blood between adjacent TIs (i.e. $S_{diff}(TI_i) - S_{diff}(TI_{i-1})$, open circle) in the same GM regions, which started to drop around TIs of 800–900 ms, reflecting a reduction in oxygenation (44–48). Although the SD is considerable, which may be due to vessel heterogeneity and relatively low SNR in the T_2 fitting, the general trend is quite clear.

Discussion

To date, most MRI techniques for quantification of absolute CBV require injection of certain exogenous contrast agents, which reportedly may cause adverse effects in elderly population and/or patients with liver or kidney problems (61). In this study, we extended the iVASO MRI approach to allow measurement of absolute arterial blood volume in physiological units (ml blood/100 ml tissue) without the need for such contrast agent administration. While the original iVASO approach (23,24), which does not include a control scan, is mainly suitable for detecting relative changes in arterial blood volume consequent to neuronal or physiological stimulations, this extended iVASO approach may find a broader range of applications in longitudinal and cross-sectional studies of brain physiology and neurovascular diseases.

Blood volume in arteries and arterioles

The term arterial blood volume is somewhat ambiguous in terms of vessel size, as it includes contributions from both the feeding arteries and the parenchymal microvasculature (arterioles). To make matters more complicated, the inflowing blood measured with iVASO, S_{diff}, may have contributions not only from macro- and micro- vessels perfusing the slice, but also from arteries that pass through the slice but occupy a fraction of the voxel and actually supply tissue in adjacent voxels. Such macrovascular contributions may lead to overestimation of regional CBV_a values, which are supposed to reflect microvascular (arterioles and small pial vessels) blood volume. As such, reported CBV_a values are by

definition “apparent” as they report on multiple vessel sizes. To suppress contamination from large arteries, crusher gradients can be applied to dephase the signal from faster flowing blood in these macrovessels (note that this is completely different from methods that label arterial blood by comparing signals with and without crusher gradients to extract CBV_a). In our experiments, crusher gradients with b-values of 0, 0.3, and 1.8 s/mm^2 were applied, corresponding to velocity encoding (V_{enc}) of infinite, 10, and 3 cm/s, respectively. The apparent GM CBV_a values decreased with crusher gradient strength (Table 3). While estimated CBV_a from scans without crusher gradients was slightly larger than most literature values, CBV_a from scans with velocity encoding for 10 cm/s was 1.27 ± 0.13 ml/100 ml, in agreement with most previous studies. The diameters of cortical arterioles have been reported to be in the range of 10–120 microns (5), and their corresponding red blood cell (RBC) velocities approximately 0.4–4 cm/s (5,62). We therefore expect that the CBV_a values from scans with V_{enc} = 3 cm/s, corresponding to vessel diameter of about 100 microns, reflect predominantly arteriolar CBV_a. Although it is generally accepted that CBV_a occupies around 20% volume of total CBV (most in Table 4), there have been a few studies (1,63) arguing that only 5–15% of parenchymal blood actually resides in arterioles. For a typical CBV_{tot} of 5.5 ml/100 ml (4), our results indicate that the actual arteriolar CBV_a is roughly 10–16% of total CBV, inline with the values reported in the studies using the QUASAR (11,40,64) and MEGESE (12) methods in Table 4. Further investigation, possibly with high resolution optical imaging in animal brains, will be needed to confirm the exact physiological origins of the measured CBV_a values with different V_{enc}.

Interestingly, the effect from the crusher gradients can also be seen in the estimated arterial transit times. The time for the inverted blood to reach the imaging slice (Δ) became longer with gradient strength, indicating the iVASO signal being sensitized to the slower flowing blood in arterioles. The time for blood to traverse the arterial compartment in the slice (δ_a) did not elevate significantly until the crusher gradient was raised to b = 1.8 s/mm^2, which is expected to be strong enough to start affecting the water diffusion in arteriolar blood. The GM Δ measured from scans with b = 1.8 s/mm^2, gap = 7 mm was consistent with previous ASL studies using similar inversion geometry (18,38). The average GM δ_a from the whole slice was shorter than that reported in visual cortex (18), which may possibly be due to transit time variations between cortices as well as to subtle discrepancies between different techniques that remain to be investigated. We then calculated the average δ_a in the posterior lobe of the slice (visual cortex) in our data to be 446 ± 35 ms (n = 11), which is significantly longer ($P < 0.01$) than the whole slice average.

Post-arterial contributions to the iVASO signal

Our simulations show that, at longer inversion times ($TI > \Delta + \delta_a$), capillary blood signal may start to contribute to the iVASO signal and the effect of exchange of water between capillaries and tissue has to be accounted for. This is done in the third term of Eq. [2a], which contains a blood flow term and extraction factor (E). At the current field strength of 3T, the blood nulling time (TI, Eq. [1]) is limited to about 1.1 s at the longest TR, and for a typical GM voxel, only scans from the 2–3 longest TIs (among all 8 TIs acquired) may be affected by inflowing capillary blood, leading to only a small contribution of capillary effects (Fig. 3b). This is reflected in the fact that f could not be reliably fitted with our data (Fig. 4c, Table 3). Again, the iVASO approach is therefore very different from many ASL techniques, where a post-labeling delay of at least 1.5 s is recommended for the inflowing blood to exchange with tissue and to generate sufficient contrast (7,30–32). When going to higher fields, blood T_1, and thus the upper TI limit becomes longer, and the iVASO approach at longer TI/TR values will become more sensitive to CBF contributions. While a proper TI/TR range where capillary effects remain negligible could still be chosen, this

would also enable iVASO to quantify CBV_a and CBF simultaneously at higher magnetic fields.

Another post-arterial contribution could potentially come from inflowing venous blood. In our experiments, the brain region from 7 mm inferior to the imaging slice and all superior areas are flipped back (Fig. 2, box 2), and limited venous blood is expected to flow in from the inferior direction. However, when only the imaging slice is flipped back (Sequence IIa in (23,24); used in (26,27)), venous label originating from superior areas can flow through the slice, which may lead to an overestimate of CBV_a. One possible way to mitigate this potential contamination is to use a venous mask, possibly at a higher resolution, to exclude voxels occupied by large veins.

Confirmation of arterial signal characteristics

The origin of the iVASO difference signal was further examined by measuring the T_2 decay of the inflowing blood. It is well known that blood T_2 is highly oxygenation level dependent. *Ex vivo* experiments with blood of normal hematocrit level (0.44) using the CPMG sequence (τ_{CPMG} = 10 ms) reported that arterial (98% O_2) and capillary (77% O_2 at baseline when assuming exponential O2 decay (46)) blood T_2 values are 138.8 and 96.6 ms, respectively (48). Our measurements (Fig. 5) show that the T_2 values of inflowing blood were within the arterial range before TI = 1000 ms, implying that S_{diff} originates primarily from arterial blood. Furthermore, the T_2 values of inflowing blood between adjacent TIs were within arterial range before TI = 700 ms, and gradually decreased into the capillary range as the inflow time (TI) gets longer, the timing of which is well in line with our measured arterial transit times ($\Delta + \delta_a \approx 800$ ms, in scans with b = 1.8 s/mm^2 in Table 3). Interestingly, our data indicates that the T_2 values have dropped slightly even before the end of arterial transit time, which implies that the oxygenation level has begun to decrease when blood reaches the pre-capillary arterioles. This observation is in line with the results reported in recent animal studies using high-resolution optical imaging techniques (65).

Technical considerations

Partial volume effects are a major concern in quantitative *in vivo* measurements. At a typical spatial resolution at 3T, a GM voxel may contain about 10–15% CSF and 3–5% WM (21). In the iVASO approach, GM tissue, WM tissue and CSF in the imaging slice are all flipped back immediately after inversion in both nulling and control scans. Therefore upon subtraction, partial volume effects should cancel out and only the inflowing arterial blood should contribute to the difference signal. One possible confounding factor may be some CSF in the inversion slab flowing into the imaging slice at TI, which would have negative magnetization at the blood nulling time because of a longer T_1 (33,34), resulting in an overestimate of CBV_a. Nevertheless, the circulation of CSF in the brain (turnaround time on the order of hours (66,67)) is rather slower than blood. As CSF has a much greater T_2 than blood and brain tissue, the measured T_2 values of the difference signal (Fig. 5) indicate that the contamination from such CSF inflow, which may increase the apparent T_2, was minimal in our data.

Another confounding factor for quantitative perfusion measurements is the BOLD effect. In iVASO, the BOLD effects in both extravascular tissue and in-slice blood are identical in nulling and control scans (flipped back) and thus subtracted out in the difference signal. The residual T_2/T_2* decay in the inflowing blood is accounted for in the fitting algorithm by adopting corresponding T_2/T_2* values for arterial and capillary compartments (Table 1) in Eq. [2]. Therefore, we expect that the contamination from the BOLD effect is minimal in our results even at relatively long TE.

In order to be of potential clinical use, extension of the proposed single-slice approach to multi-slice or 3D would be important. This seems difficult in view of the transit time dependence of the measured difference signal. In order to estimate the effect of transit time, the gap between imaging slice and inversion slab was varied to evaluate its influence on S_{diff} and the fitted parameters. The measured CBV_a values and transit times (Δ, δ_a) (Table 3) were not significantly different between the two experiments. Note that the mean of Δ in Table 3 did increase slightly for gap = 17 mm, but the difference was not statistically different in our data. This trend of limited effect on perfusion measurements of longer inflow delays in large vessels was also observed in the literature data summarized in Table 5. This is logical as the inflowing blood is mainly in fast-flowing large arteries before it reaches the cortical region that it supplies. Therefore effective increases in the gap that occur when measuring blood volume in slices located more superior in the brain are expected to have only a small effect on Δ and no substantial influence on the fitted CBV_a and δ_a values. This important observation indicates that it should be feasible to extend the current method from single slice to 3D by incorporating a different readout sequence such as 3D gradient spin echo (GraSE), in a way similar to some ASL (68,69) and VASO (70,71) approaches.

The current protocol for this method, in which eight TR/TI combinations were acquired to fit CBV_a, Δ, δ_a, f, took about 10 minutes. While such a scan duration is reasonable in this methodology study, it can be shortened markedly and tailored according to specific situations for clinical application. For instance, the scans for $TI < \Delta$ are not necessary, as S_{diff} will be largely within noise range. The number of TIs and intervals between them (not necessarily equidistant) can be optimized for particular applications by using a priori knowledge of parameter distributions (17,72) or adaptive sequential design methods (73). An alternative approach may be to acquire a low resolution arterial transit time map first by performing iVASO or ASL scans with fewer repetitions (74). It has been demonstrated that the arterial transit times within most cortical regions only have small variations (40). Therefore a spatial resolution much coarser than 3 mm isotropic (typical at 3T) may be sufficient to capture most information. CBV_a can then be quantified with a single TI using Eq. [2], or more accurately, with multiple TIs of $\Delta \leq TI \leq \Delta + \delta_a$. Note that partial volume effects with WM at lower resolution will not affect the results, as long as TI is shorter than WM Δ so that little inverted blood water has reach WM.

Conclusions

We presented a MRI technique for quantifying absolute arterial CBV in physiological units (ml blood/100ml tissue) without the need for exogenous contrast agent injection. In this approach, the amount of inflowing blood was measured at a series of inversion times (TI), from which CBV_a as well as arterial transit times could be quantified on a voxel-by-voxel basis. Furthermore, by incorporating crusher gradients in *both* nulling and control scans, the signal could be sensitized predominantly to parenchymal CBV_a. The measured GM CBV_a and arterial transit time values were in agreement with reported literature values. The arterial origin of the difference signal in our method was validated by measuring its T_2 relaxation. This approach provides a useful alternative to existing blood volume techniques for mapping absolute CBV_a in normal subjects and patients with altered tissue perfusion.

Acknowledgments

The authors thank Dr. Hanzhang Lu at University of Texas Southwestern Medical Center for stimulating discussions, and Mr. Joseph S. Gillen, Ms. Terri Brawner, Ms. Kathleen Kahl, and Ms. Ivana Kusevic at Johns Hopkins University and Kennedy Krieger Institute for experimental assistance. This publication was made possible by grant support from NIH-NIBIB R01-EB004130, EB002634 and NIH-NCRR P41-RR015241. The National Center for Research Resources (NCRR) is a component of the National Institutes of Health (NIH). The contents of the paper are solely the responsibility of the authors and do not necessarily represent the official view of NCRR or

NIH. Equipment used in the study is manufactured by Philips. Dr. van Zijl is a paid lecturer for Philips Medical Systems and the inventor of technology that is licensed to Philips. This arrangement has been approved by Johns Hopkins University in accordance with its conflict of interest policies.

Grant support from NIH-NIBIB R01-EB004130 and NIH-NCRR P41-RR015241.

Abbreviations used

CBV	cerebral blood volume
GM	grey matter
WM	white matter
ASL	arterial spin labeling
VASO	vascular-space-occupancy
iVASO	inflow VASO
CBF	cerebral blood flow
CSF	cerebrospinal fluid
SD	standard deviation
SNR	signal-to-noise ratio
CNR	contrast-to-noise ratio

References

1. Mchedlishvili, G. Arterial Behavior and Blood Circulation in the Brain. New York: Plenum Press; 1986.
2. Auer LM, Johansson BB. Dilatation of pial arterial vessels in hypercapnia and in acute hypertension. Acta Physiol Scand. 1980; 109(3):249–251. [PubMed: 7446169]
3. Mchedlishvili GI, Baramidze DG, Nicolaishvili LS, Mamisashvili VA. Vascular mechanisms responsible for microcirculation of the cerebral cortex. Biochem Exp Biol. 1974–75; 11:113–129.
4. Lu H, Law M, Johnson G, Ge Y, van Zijl PC, Helpern JA. Novel approach to the measurement of absolute cerebral blood volume using vascular-space-occupancy magnetic resonance imaging. Magn Reson Med. 2005; 54(6):1403. [PubMed: 16254955]
5. Sharan M, DJM, Koehler RC, Traystman RJ, Popel AS. A compartmental model for oxygen transport in brain microcirculation. Ann Biomed Eng. 1989; 17(1):13. [PubMed: 2919811]
6. Le Bihan D, Breton E, Lallemand D, Aubin ML, Vignaud J, Laval-Jeantet M. Separation of diffusion and perfusion in intravoxel incoherent motion MR imaging. Radiology. 1988; 168(2):497. [PubMed: 3393671]
7. Silva AC, Williams DS, Koretsky AP. Evidence for the exchange of arterial spin-labeled water with tissue water in rat brain from diffusion-sensitized measurements of perfusion. Magn Reson Med. 1997; 38(2):232–237. [PubMed: 9256102]
8. Duong TQ, Kim SG. In vivo MR measurements of regional arterial and venous blood volume fractions in intact rat brain. Magn Reson Med. 2000; 43(3):393. [PubMed: 10725882]
9. Barbier EL, Silva AC, Kim SG, Koretsky AP. Perfusion imaging using dynamic arterial spin labeling (DASL). Magn Reson Med. 2001; 45(6):1021. [PubMed: 11378880]
10. Kim T, Kim SG. Quantification of cerebral arterial blood volume using arterial spin labeling with intravoxel incoherent motion-sensitive gradients. Magn Reson Med. 2006; 55(5):1047. [PubMed: 16596632]
11. Petersen ET, Lim T, Golay X. Model-free arterial spin labeling quantification approach for perfusion MRI. Magn Reson Med. 2006; 55(2):219. [PubMed: 16416430]
12. An H, Lin W. Cerebral venous and arterial blood volumes can be estimated separately in humans using magnetic resonance imaging. Magn Reson Med. 2002; 48(4):583. [PubMed: 12353273]

13. An H, Lin W. Cerebral oxygen extraction fraction and cerebral venous blood volume measurements using MRI: effects of magnetic field variation. Magn Reson Med. 2002; 47(5):958. [PubMed: 11979575]
14. Stefanovic B, Pike GB. Venous refocusing for volume estimation: VERVE functional magnetic resonance imaging. Magn Reson Med. 2005; 53(2):339–347. [PubMed: 15678548]
15. Ito H, Kanno I, Iida H, Hatazawa J, Shimosegawa E, Tamura H, Okudera T. Arterial fraction of cerebral blood volume in humans measured by positron emission tomography. Ann Nucl Med. 2001; 15(2):111. [PubMed: 11448068]
16. Kim T, Kim SG. Quantification of cerebral arterial blood volume and cerebral blood flow using MRI with modulation of tissue and vessel (MOTIVE) signals. Magn Reson Med. 2005; 54(2):333. [PubMed: 16032688]
17. Brookes MJ, Morris PG, Gowland PA, Francis ST. Noninvasive measurement of arterial cerebral blood volume using Look-Locker EPI and arterial spin labeling. Magn Reson Med. 2007; 58(1): 41. [PubMed: 17659615]
18. Francis ST, Bowtell R, Gowland PA. Modeling and optimization of look-locker spin labeling for measuring perfusion and transit time changes in activation studies taking into account arterial blood volume. Magn Reson Med. 2008; 59(2):316. [PubMed: 18183614]
19. Vazquez AL, Lee GR, Hernandez-Garcia L, Noll DC. Application of selective saturation to image the dynamics of arterial blood flow during brain activation using magnetic resonance imaging. Magn Reson Med. 2006; 55(4):816–825. [PubMed: 16506156]
20. Lu H, Golay X, Pekar JJ, van Zijl PC. Functional magnetic resonance imaging based on changes in vascular space occupancy. Magn Reson Med. 2003; 50(2):263. [PubMed: 12876702]
21. Donahue MJ, Lu H, Jones CK, Edden RA, Pekar JJ, van Zijl PC. Theoretical and experimental investigation of the VASO contrast mechanism. Magn Reson Med. 2006; 56(6):1261. [PubMed: 17075857]
22. Hua J, Donahue MJ, Zhao JM, Grgac K, Huang AJ, Zhou J, van Zijl PC. Magnetization transfer enhanced vascular-space-occupancy (MT-VASO) functional MRI. Magn Reson Med. 2009; 61(4): 944. [PubMed: 19215043]
23. Hua, J.; Qin, Q.; Donahue, MJ.; Zhou, J.; Pekar, J.; van Zijl, PCM. Functional MRI Using Arteriolar Cerebral Blood Volume Changes. Proc 17th Annual Meeting ISMRM; 2009; Hawaii, USA. p. 12
24. Hua J, Qin Q, Donahue MJ, Zhou J, Pekar JJ, van Zijl PC. Inflow-based Vascular-Space-Occupancy (iVASO) MRI. Magn Reson Med. in press.
25. Hua, J.; Qin, Q.; Pekar, J.; van Zijl, PCM. Measuring Absolute Arteriolar Cerebral Blood Volume (CBVa) in Human Brain Gray Matter (GM) without Contrast Agent. Proc 17th Annual Meeting ISMRM; 2009; Hawaii, USA. p. 5314
26. Donahue MJ, Sideso E, MacIntosh BJ, Kennedy J, Handa A, Jezzard P. Absolute arterial cerebral blood volume quantification using inflow vascular-space-occupancy with dynamic subtraction magnetic resonance imaging. J Cereb Blood Flow Metab. 2010; 30(7):1329–1342. [PubMed: 20145656]
27. Donahue, MJ.; MacIntosh, BJ.; Sideso, E.; Bright, M.; Kennedy, J.; Handa, A.; Jezzard, P. Absolute cerebral blood volume (CBV) quantification without contrast agents using inflow vascular-space-occupancy (iVASO) with dynamic subtraction. Proc 17th Annual Meeting ISMRM; 2009; Hawaii, USA. p. 628
28. Detre JA, Leigh JS, Williams DS, Koretsky AP. Perfusion imaging. Magn Reson Med. 1992; 23(1):37. [PubMed: 1734182]
29. Williams DS, Detre JA, Leigh JS, Koretsky AP. Magnetic resonance imaging of perfusion using spin inversion of arterial water. Proc Natl Acad Sci U S A. 1992; 89(1):212. [PubMed: 1729691]
30. Alsop DC, Detre JA. Reduced transit-time sensitivity in noninvasive magnetic resonance imaging of human cerebral blood flow. J Cereb Blood Flow Metab. 1996; 16(6):1236. [PubMed: 8898697]
31. Ye FQ, Mattay VS, Jezzard P, Frank JA, Weinberger DR, McLaughlin AC. Correction for vascular artifacts in cerebral blood flow values measured by using arterial spin tagging techniques. Magn Reson Med. 1997; 37(2):226. [PubMed: 9001147]

32. Donahue MJ, Lu H, Jones CK, Pekar JJ, van Zijl PC. An account of the discrepancy between MRI and PET cerebral blood flow measures. A high-field MRI investigation NMR Biomed. 2006; 19(8):1043–1054.
33. Lu H, Clingman C, Golay X, van Zijl PC. Determining the longitudinal relaxation time (T1) of blood at 3.0 Tesla. Magn Reson Med. 2004; 52(3):679. [PubMed: 15334591]
34. Lu H, Nagae-Poetscher LM, Golay X, Lin D, Pomper M, van Zijl PC. Routine clinical brain MRI sequences for use at 3.0 Tesla. J Magn Reson Imaging. 2005; 22(1):13. [PubMed: 15971174]
35. Wu WC, Buxton RB, Wong EC. Vascular space occupancy weighted imaging with control of residual blood signal and higher contrast-to-noise ratio. IEEE Trans Med Imaging. 2007; 26(10): 1319. [PubMed: 17948723]
36. Lu, H. Magnetization “reset” for non-steady-state blood spins in Vascular-Space-Occupancy (VASO) fMRI. Proc 16th Annual Meeting ISMRM; 2008; Toronto, Canada. p. 406
37. Gonzalez-At JB, Alsop DC, Detre JA. Cerebral perfusion and arterial transit time changes during task activation determined with continuous arterial spin labeling. Magn Reson Med. 2000; 43(5): 739. [PubMed: 10800040]
38. Hendrikse J, Lu H, van der Grond J, Van Zijl PC, Golay X. Measurements of cerebral perfusion and arterial hemodynamics during visual stimulation using TURBO-TILT. Magn Reson Med. 2003; 50(2):429. [PubMed: 12876722]
39. Wang J, Alsop DC, Song HK, Maldjian JA, Tang K, Salvucci AE, Detre JA. Arterial transit time imaging with flow encoding arterial spin tagging (FEAST). Magn Reson Med. 2003; 50(3):599. [PubMed: 12939768]
40. Hendrikse J, Petersen ET, van Laar PJ, Golay X. Cerebral border zones between distal end branches of intracranial arteries: MR imaging. Radiology. 2008; 246(2):572. [PubMed: 18055872]
41. Silva AC, Zhang W, Williams DS, Koretsky AP. Estimation of water extraction fractions in rat brain using magnetic resonance measurement of perfusion with arterial spin labeling. Magn Reson Med. 1997; 37(1):58–68. [PubMed: 8978633]
42. Francis ST, Pears JA, Butterworth S, Bowtell RW, Gowland PA. Measuring the change in CBV upon cortical activation with high temporal resolution using look-locker EPI and Gd-DTPA. Magn Reson Med. 2003; 50(3):483. [PubMed: 12939755]
43. Liu P, Uh J, Lu H. Determination of spin compartment in arterial spin labeling MRI. Magn Reson Med;n/a. 10.1002/mrm.22601
44. Wright GA, Hu BS, Macovski A. 1991 I.I. Rabi Award. Estimating oxygen saturation of blood in vivo with MR imaging at 1.5 T. J Magn Reson Imaging. 1991; 1(3):275–283. [PubMed: 1802140]
45. Ogawa S, Menon RS, Tank DW, Kim SG, Merkle H, Ellermann JM, Ugurbil K. Functional brain mapping by blood oxygenation level-dependent contrast magnetic resonance imaging. A comparison of signal characteristics with a biophysical model. Biophys J. 1993; 64(3):803. [PubMed: 8386018]
46. Zhao JM, Clingman CS, Narvainen MJ, Kauppinen RA, van Zijl PC. Oxygenation and hematocrit dependence of transverse relaxation rates of blood at 3T. Magn Reson Med. 2007; 58(3):592. [PubMed: 17763354]
47. Chen JJ, Pike GB. Human whole blood T2 relaxometry at 3 Tesla. Magn Reson Med. 2009; 61(2): 249–254. [PubMed: 19165880]
48. Qin Q, Grgac K, van Zijl PC. Determination of whole-brain oxygen extraction fractions by fast measurement of blood T2 in the jugular vein. Magn Reson Med. 2010 in press.
49. Thulborn KR, Waterton JC, Matthews PM, Radda GK. Oxygenation dependence of the transverse relaxation time of water protons in whole blood at high field. Biochim Biophys Acta. 1982; 714(2):265–270. [PubMed: 6275909]
50. Bryant RG, Marill K, Blackmore C, Francis C. Magnetic relaxation in blood and blood clots. Magn Reson Med. 1990; 13(1):133–144. [PubMed: 2319929]
51. Brittain JH, Hu BS, Wright GA, Meyer CH, Macovski A, Nishimura DG. Coronary angiography with magnetization-prepared T2 contrast. Magn Reson Med. 1995; 33(5):689–696. [PubMed: 7596274]

52. Lu H, Zhao C, Ge Y, Lewis-Amezcua K. Baseline blood oxygenation modulates response amplitude: Physiologic basis for intersubject variations in functional MRI signals. Magn Reson Med. 2008; 60(2):364–372. [PubMed: 18666103]
53. Lu H, Ge Y. Quantitative evaluation of oxygenation in venous vessels using T2-Relaxation-Under-Spin-Tagging MRI. Magn Reson Med. 2008; 60(2):357–363. [PubMed: 18666116]
54. Botnar RM, Stuber M, Danias PG, Kissinger KV, Manning WJ. Improved coronary artery definition with T2-weighted, free-breathing, three-dimensional coronary MRA. Circulation. 1999; 99(24):3139–3148. [PubMed: 10377077]
55. Woods RP, Grafton ST, Holmes CJ, Cherry SR, Mazziotta JC. Automated image registration: I. General methods and intrasubject, intramodality validation. J Comput Assist Tomo. 1998; 22(1): 139.
56. Lu H, Donahue MJ, van Zijl PC. Detrimental effects of BOLD signal in arterial spin labeling fMRI at high field strength. Magn Reson Med. 2006; 56(3):546–552. [PubMed: 16894581]
57. van Gelderen P, de Zwart JA, Duyn JH. Pittfalls of MRI measurement of white matter perfusion based on arterial spin labeling. Magn Reson Med. 2008; 59(4):788. [PubMed: 18383289]
58. van Osch MJ, Teeuwisse WM, van Walderveen MA, Hendrikse J, Kies DA, van Buchem MA. Can arterial spin labeling detect white matter perfusion signal? Magn Reson Med. 2009; 62(1):165–173. [PubMed: 19365865]
59. Grandin CB, Bol A, Smith AM, Michel C, Cosnard G. Absolute CBF and CBV measurements by MRI bolus tracking before and after acetazolamide challenge: repeatabilily and comparison with PET in humans. Neuroimage. 2005; 26(2):525–535. [PubMed: 15907309]
60. Rostrup E, Knudsen GM, Law I, Holm S, Larsson HB, Paulson OB. The relationship between cerebral blood flow and volume in humans. Neuroimage. 2005; 24(1):1–11. [PubMed: 15588591]
61. Boyd AS, Zic JA, Abraham JL. Gadolinium deposition in nephrogenic fibrosing dermopathy. J Am Acad Dermatol. 2007; 56(1):27–30. [PubMed: 17109993]
62. Kobari M, Gotoh F, Fukuuchi Y, Tanaka K, Suzuki N, Uematsu D. Blood flow velocity in the pial arteries of cats, with particular reference to the vessel diameter. J Cereb Blood Flow Metab. 1984; 4(1):110–114. [PubMed: 6693510]
63. Tomita M, Gotoh F, Amano T, Tanahashi N, Kobari M, Shinohara T, Mihara B. Transfer function through regional cerebral cortex evaluated by a photoelectric method. Am J Physiol. 1983; 245(3):H385–398. [PubMed: 6614188]
64. Petersen ET, Mouridsen K, Golay X. The QUASAR reproducibility study, Part II: Results from a multi-center Arterial Spin Labeling test-retest study. Neuroimage. 2010; 49(1):104–113. [PubMed: 19660557]
65. Hillman EM, Devor A, Bouchard MB, Dunn AK, Krauss GW, Skoch J, Bacskai BJ, Dale AM, Boas DA. Depth-resolved optical imaging and microscopy of vascular compartment dynamics during somatosensory stimulation. Neuroimage. 2007; 35(1):89. [PubMed: 17222567]
66. Di Chiro G. Observations on the circulation of the cerebrospinal fluid. Acta Radiol Diagn (Stockh). 1966; 5:988. [PubMed: 5297333]
67. Haaxma-Reiche H, Piers A, Beekhuis H. Normal cerebrospinal fluid dynamics. A study with intraventricular injection of 111In-DTPA in leukemia and lymphoma without meningeal involvement. Arch Neurol. 1989; 46(9):997. [PubMed: 2775015]
68. Gunther M, Oshio K, Feinberg DA. Single-shot 3D imaging techniques improve arterial spin labeling perfusion measurements. Magn Reson Med. 2005; 54(2):491–498. [PubMed: 16032686]
69. MacIntosh BJ, Pattinson KT, Gallichan D, Ahmad I, Miller KL, Feinberg DA, Wise RG, Jezzard P. Measuring the effects of remifentanil on cerebral blood flow and arterial arrival time using 3D GRASE MRI with pulsed arterial spin labelling. J Cereb Blood Flow Metab. 2008; 28(8):1514–1522. [PubMed: 18506198]
70. Poser BA, Norris DG. 3D single-shot VASO using a Maxwell gradient compensated GRASE sequence. Magn Reson Med. 2009; 62(1):255. [PubMed: 19319900]
71. Donahue MJ, Blicher JU, Ostergaard L, Feinberg DA, Macintosh BJ, Miller KL, Gunther M, Jezzard P. Cerebral blood flow, blood volume, and oxygen metabolism dynamics in human visual and motor cortex as measured by whole-brain multi-modal magnetic resonance imaging. J Cereb Blood Flow Metab. 2009; 29(11):1856–1866. [PubMed: 19654592]

72. Xie J, Gallichan D, Gunn RN, Jezzard P. Optimal design of pulsed arterial spin labeling MRI experiments. Magn Reson Med. 2008; 59(4):826–834. [PubMed: 18302248]

73. Xie J, Clare S, Gallichan D, Gunn RN, Jezzard P. Real-time adaptive sequential design for optimal acquisition of arterial spin labeling MRI data. Magn Reson Med. 2010; 64(1):203–210. [PubMed: 20572144]

74. Dai, W.; Robson, PM.; Shankaranarayanan, A.; Alsop, DC. ASL Perfusion Measurement Using a Rapid, Low Resolution Arterial Transit Time Prescan. Proc 17th Annual Meeting ISMRM; 2009; Hawaii, USA. p. 624

75. Herscovitch P, Raichle ME. What is the correct value for the brain--blood partition coefficient for water? J Cereb Blood Flow Metab. 1985; 5(1):65. [PubMed: 3871783]

76. Hutchinson EB, Stefanovic B, Koretsky AP, Silva AC. Spatial flow-volume dissociation of the cerebral microcirculatory response to mild hypercapnia. Neuroimage. 2006; 32(2):520–530. [PubMed: 16713717]

77. Stefanovic B, Hutchinson E, Yakovleva V, Schram V, Russell JT, Belluscio L, Koretsky AP, Silva AC. Functional reactivity of cerebral capillaries. J Cereb Blood Flow Metab. 2008; 28(5):961–972. [PubMed: 18059431]

78. Ito H, Ibaraki M, Kanno I, Fukuda H, Miura S. Changes in the arterial fraction of human cerebral blood volume during hypercapnia and hypocapnia measured by positron emission tomography. J Cereb Blood Flow Metab. 2005; 25(7):852. [PubMed: 15716851]

79. Lee SP, Duong TQ, Yang G, Iadecola C, Kim SG. Relative changes of cerebral arterial and venous blood volumes during increased cerebral blood flow: implications for BOLD fMRI. Magn Reson Med. 2001; 45(5):791. [PubMed: 11323805]

80. Kim T, Hendrich KS, Masamoto K, Kim SG. Arterial versus total blood volume changes during neural activity-induced cerebral blood flow change: implication for BOLD fMRI. J Cereb Blood Flow Metab. 2007; 27(6):1235. [PubMed: 17180136]

81. Kety SS, Schmidt CF. The Nitrous Oxide Method For The Quantitative Determination Of Cerebral Blood Flow In Man: Theory, Procedure And Normal Values. J Clin Invest. 1948; 27(4):476–483.

APPENDIX

Here we derive the analytical solution for the difference signal (S_{diff}) between control and nulling scans in Eq. [2] when $\Delta + \delta_a < TI \leq \Delta + \delta_a + \delta_c$, as the sum of three contributions (all parameters have been defined in Eq. [2] and Table 1):

a. the arterial compartment

The inverted blood water spins have perfused the entire arterial compartment at this TI range. Using the equations derived in Hua et al. (23,24), the difference signal in this compartment can be written as:

$$S_{diff}^{art} = M_0 \cdot C_b \cdot CBV_a \cdot (1 - e^{-TR/T_{1,a}}) \cdot e^{-TE/T_{2,a}^*} \quad [A1]$$

b. intravascular capillary compartment

A fraction (1-E) of the inflowing blood water protons will remain in the capillaries at TI. The longitudinal magnetization of these protons undergoes the inversion recovery process as in a conventional VASO sequence, which is governed by the following Bloch equation:

$$\frac{dM_z}{dt} = -\frac{M_z - M_0}{T_{1,blood}} \quad [A2]$$

Note that before and after $\Delta + \delta_a$, it relaxes with $T_{1,a}$ and $T_{1,c}$, respectively. The longitudinal magnetization of the inflowing blood at TI in the nulling and control scans can be derived as:

$$M_{z,null}(TI)=M_0 \cdot \left(1 - e^{TI_{ex} \cdot (1/T_{1,a} - 1/T_{1,c})}\right) \quad [A3]$$

$$M_{z,ctrl}(TI)=M_0 \cdot \left(1 - e^{-TR/T_{1,a} + TI_{ex} \cdot (1/T_{1,a} - 1/T_{1,c})}\right) \quad [A4]$$

respectively, where $TI_{ex} = TI - \Delta - \delta_a$. Thus the difference signal in this compartment can be written as:

$$\begin{aligned} S_{diff}^{cap-non-exch} &= C_b \cdot (1 - E) \cdot f \cdot TI_{ex} \cdot (M_{z,ctrl}(TI) - M_{z,null(TI)}) \cdot e^{-TE/T_{2,c}^*} \\ &= M_0 \cdot C_b \cdot (1 - E) \cdot f \cdot TI_{ex} \cdot e^{TI_{ex} \cdot (1/T_{1,a} - 1/T_{1,c})} (1 - e^{-TR/T_{1,a}}) \cdot e^{-TE/T_{2,c}^*} \end{aligned} \quad [A5]$$

c. the extravascular tissue compartment

A fraction (E) of the inflowing blood water protons will diffuse out of the vasculature and exchange with extravascular tissue water protons in the capillary bed. The longitudinal magnetization of the extravascular tissue can be described by the well-known flow-modified Bloch equation (well-mixed single compartment model) (81):

$$\frac{dM_z}{dt} = -\frac{M_z - M_0}{T_{1,t}} + f \cdot \left[M_{blood} - \frac{M_z}{\lambda}\right] \quad [A6]$$

in which M_z represents the tissue (not blood) magnetization. In the nulling and control scans, the inflowing blood magnetization can be written as:

$$M_{blood,null} = \frac{M_0}{\lambda} \cdot \left(1 - e^{-(t-\Delta-\delta_a)/T_{1,c} + TI_{ex}/T_{1,a}}\right) \quad [A7]$$

$$M_{blood,ctrl} = \frac{M_0}{\lambda} \cdot \left(1 - e^{-(t-\Delta-\delta_a)/T_{1,c} + (TI_{ex}-TR)/T_{1,a}}\right) \quad [A8]$$

respectively. Eq. [A6] can be solved with M_{blood} from Eqs. [A7,8] for the nulling and control scans:

$$M_{z,null}(TI)=M_0 \cdot [1 - \left(\frac{E \cdot f}{\lambda} / \left(\frac{1}{T_{1,app}} - \frac{1}{T_{1,c}}\right)\right) \cdot \left(e^{-TI_{ex}/T_{1,c}} - e^{-TI_{ex}/T_{1,app}}\right) \cdot e^{TI_{ex}/T_{1,a}} - e^{-TI_{ex}/T_{1,app} + (TI_{ex}-TR)/T_{1,t}}] \quad [A9]$$

$$M_{z,ctrl}(TI)=M_0\cdot\left[1-\left(\frac{E\cdot f}{\lambda}/\left(\frac{1}{T_{1,app}}-\frac{1}{T_{1,c}}\right)\right)\cdot\left(e^{-TI_{ex}/T_{1,c}}-e^{-TI_{ex}/T_{1,app}}\right)\cdot e^{(TI_{ex}-TR)/T_{1,a}}-e^{-TI_{ex}/T_{1,app}+(TI_{ex}-TR)/T_{1,t}}\right]$$

[A10]

respectively. The difference signal in this compartment can then be written as:

$$\begin{aligned}S_{diff}^{cap-exch}&=C_t\cdot\left(M_{z,ctrl}(TI)-M_{z,null}(TI)\right)\cdot e^{-TE/T_{2,t}^*}\\&=M_0\cdot C_t\cdot\left(\frac{E\cdot f}{\lambda}/\left(\frac{1}{T_{1,app}}-\frac{1}{T_{1,c}}\right)\right)\cdot\left(e^{-TI_{ex}/T_{1,c}}-e^{-TI_{ex}/T_{1,app}}\right)\cdot e^{TI_{ex}/T_{1,a}}\cdot\left(1-e^{-TR/T_{1,a}}\right)\cdot e^{-TE/T_{2,t}^*}\end{aligned}$$

[A11]

All above analytical solutions have been verified by comparing with the numerical simulations using the corresponding Bloch equations.

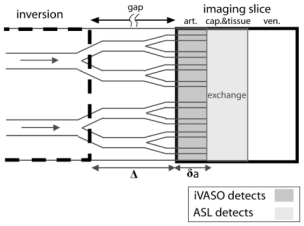

Fig. 1.

Illustration of the different principles employed between iVASO and pulsed ASL. Blood flowing into the vascular tree is inverted (dashed box), after which Δ is the time needed for inverted blood to traverse the gap between inversion and image plane (solid box) and δa the time needed for blood to traverse the arterial compartment before reaching capillaries. The sum, $\Delta + \delta_a$, is defined as the arterial transit time. In view of the impermeability of arterial vessels, it is assumed that blood water predominantly exchanges with tissue water in the capillary bed. The major difference between the contrast mechanisms is that iVASO is designed to highlight the vascular signal in the arterial and arteriolar compartments by nulling arterial blood while keeping full signal in others, whereas ASL is sensitized to perfusion by monitoring labeled spins that have exchanged from the capillary compartment to extravascular tissue.

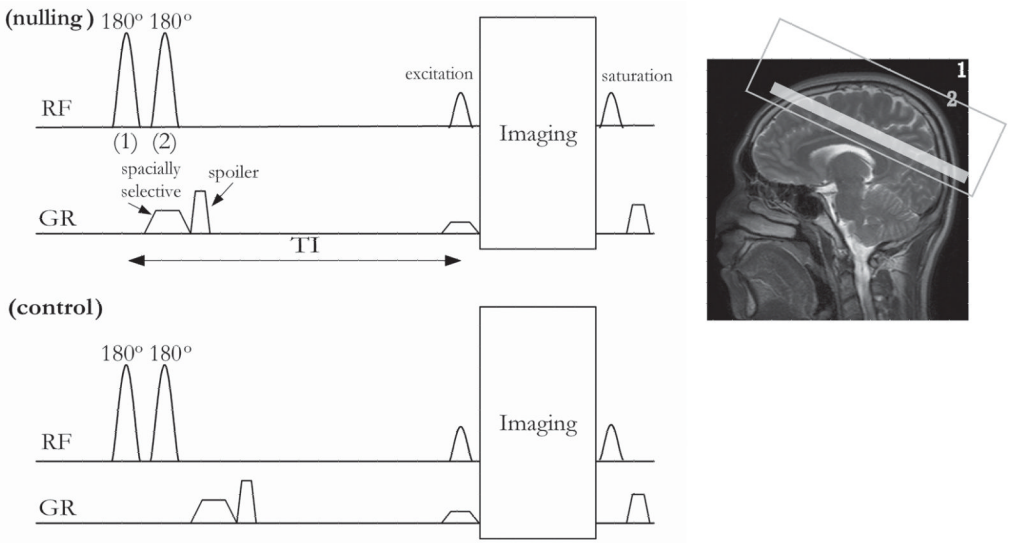

Fig. 2.

Pulse sequence for measuring CBV_a, consisting of nulling (left, top) and control (left, bottom) acquisitions. “RF” and “GR” stand for radio frequency and gradient pulses, respectively. The spatially selective inversion geometry in the nulling scan is illustrated on the right, with the light-gray shaded box indicating the imaging slice. In the nulling scan, a spatially non-selective inversion (black box labeled “1”) is followed by slab-selective flip-back (light-gray box labeled “2”) covering the imaging slice and the superior brain to minimize possible inflowing venous blood. A spoiler gradient is applied after the inversion pulses to eliminate residual transverse magnetization. Imaging is initiated at TI, which is followed by a spatially non-selective saturation pulse to achieve steady state (see Methods).

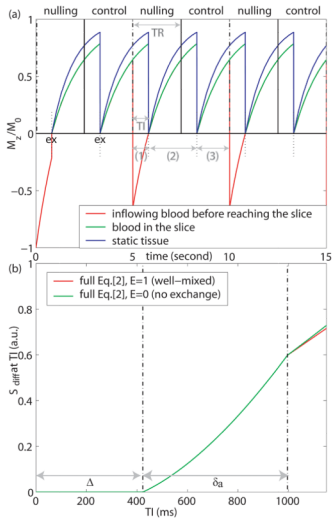

Fig. 3.

(a) Bloch equation simulation of the signal evolution for inflowing blood before reaching the slice (red), blood in the slice (green) and static tissue (blue) for a series of interleaved nulling and control scans. The inversion pulses of the first nulling scan start from time = 0 s. The dash dot and solid vertical lines represent the inversion pulses in the nulling and control scans, respectively. The short dotted vertical lines indicate the excitation pulse (marked as "ex") at the beginning of the image acquisition module. A spatially non-selective saturation pulse applied immediately after each imaging module sets all blood signals to zero to achieve a steady state (see Methods). **(b)** Simulation of the difference signal between control and nulling scans (S_{diff}) as a function of TI (Eq. [2]), assuming: (i) a well-mixed capillary compartment (E=1) (red); (ii) no water exchange between blood and tissue in the capillary compartment (E=0) (green). Typical literature values (Table 1) were used for both simulations.

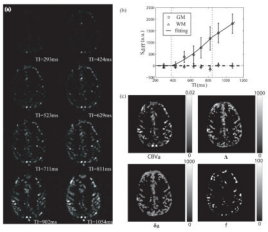

Fig. 4.

Representative results for one subject: **(a)** Difference images for each TI in arbitrary units (a.u.). **(b)** Average S_{diff} (a.u.) in GM and WM as a function of TI. The error bars represent the standard deviations across the slice, which may have substantial variations in view of the vessel heterogeneity in different cortical regions. The mean GM curve was fitted with Eq. [2]. The two vertical dotted lines depict the fitted Δ and Δ + δ_a. **(c)** Fitted maps of *CBVa*, Δ, δa, *f* in units of ml/100 ml, ms, ms and ml/100 ml/min, respectively. It can be seen that the fitting is not quite sensitive to f at the current field strength. For this data set, the gap between inversion and slice was 7 mm, and crusher gradients of b = 0.3 s/mm^2 were applied.

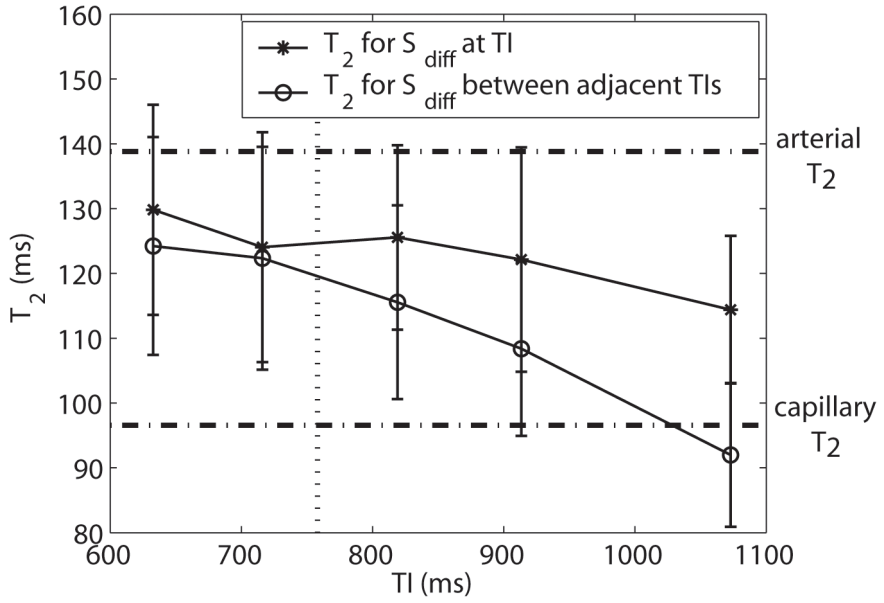

Fig. 5.

Measured T_2 values in GM of all inflowing blood at a certain TI (asterisk) and for blood representing the difference between adjacent TIs (open circle; e.g. T_2 at TI = 629 ms is from the blood that flows in between TI = 523 and 629 ms, i.e. $S_{diff}(TI=629)-S_{diff}(TI=523)$). Note that only TIs longer than 600 ms were included to allow sufficient inflowing blood in GM. The two horizontal dash-dot lines indicate the T_2 values for arterial (98% O_2, 138.8 ms) and capillary (77% O_2 at baseline when assuming exponential O2 decay (46), 96.6 ms) blood with normal hematocrit level (0.44) reported from *ex vivo* measurements using CPMG sequence ($\tau CPMG$ = 10 ms) (48). The vertical dotted line depicts the average arterial transit time ($\Delta + \delta_a$) measured in our data (Table 3). Mean values in GM were calculated per subject and then averaged across subjects (n = 5; error bars represent inter-subject SDs). For these experiments, the gap between inversion and imaging slice was 7 mm and crusher gradients of b = 1.8 s/mm^2 were applied.

Table 1

Summary of parameters in Eq. [2]. The values cited for all physiological parameters are for GM, unless otherwise mentioned.

Parameter	Physiological and Physical Meaning	Units	Literature Values
CBV_a	arterial cerebral blood volume	ml of blood/ml of brain	1.1 (5)
Δ^{+}	delivery time for the leading edge of the inverted blood to reach the imaging slice (see Figs. 1, 3)	s	0.423 (18)
δ_a +	mean time for blood to traverse the arterial compartment before entering the capillaries (see Figs. 1,3)	s	0.573 (18)
f	cerebral blood flow, or perfusion rate	ml of blood/ml of brain/s	0.92×10^{-2} (21) (55 ml/100 ml/min)
M_0	a constant giving the MR signal per unit volume of water protons at equilibrium	a.u.	N/A
E	extraction fraction for water	unitary	0.5 (41)
C_b	blood water proton density	ml water/ml blood	0.87 (75)
C_t	tissue water proton density	ml water/ml tissue	0.89 for GM (75), 0.73 for WM (75)
$T_{1,a}$	longitudinal relaxation time of arterial blood	s	1.627 (33) @ 3T ++
$T_2^*{}_{,a}$	transverse relaxation time of arterial blood	s	54.9×10^{-3} (46) @ 3T
$T_{1,c}$	longitudinal relaxation time of capillary blood	s	1.627 (33) @ 3T ++
$T_2^*{}_{,c}$	transverse relaxation time of capillary blood	s	30.5×10^{-3} (46) @ 3T +++
δ_c	mean time for blood to traverse the capillary compartment	s	0.5–1 (76,77)
λ	brain-blood partition coefficient	ml/g	0.9 (75)

+ The sum of the two ($\Delta + \delta_a$) is defined as the arterial transit time (17,18,30).

++ The same T_1 values were assumed for all vascular compartments in view of the small differences at 3T (33) (see Theory).

+++ An exponential decay of oxygenation level was assumed in capillaries. Therefore the average capillary oxygenation level was taken to be 77% (46).

Table 2

GM SNR for nulling (SNR_{null}) and control (SNR_{ctrl}) scans and resulting CNR for the difference signal (S_{diff}).

TR (ms)	5000	3100	2500	2000	1667	1300	1000	650
NSA	10	15	15	18	18	30	40	70
SNR_{null}	377 ± 67	348 ± 76	344 ± 71	333 ± 64	334 ± 54	385 ± 39	309 ± 66	402 ± 45
SNR_{ctrl}	331 ± 55	382 ± 64	329 ± 67	368 ± 58	392 ± 73	387 ± 38	307 ± 55	377 ± 39
CNR	11.2 ± 4.3	10.8 ± 4.7	11.8 ± 4.3	10.6 ± 3.6	11.6 ± 3.7	12.4 ± 4.2	11.0 ± 3.6	12.1 ± 4.0

Results for one subject (gap = 7 mm, b = 0.3 s/mm^2). Comparable results were observed in all subjects.

CNR is defined as $\frac{S_{ctrl} - S_{null}}{noise} \cdot \sqrt{NSA}$.

SNR and CNR were calculated on voxel-by-voxel basis before averaging over GM voxels.

NSA: number of signals averaged.

Table 3

Average GM values (n = 11) of CBV_a, Δ, δ_a, f from the fitted maps.

Crusher b value (s/mm^2)	Gap* (mm)	CBV_a (ml/100ml)	Δ (ms)	δ_a (ms)	f$^+$	
					(ml/100 ml/min)	(ml/ml/s)
0	**7**	2.04 ± 0.27	315 ± 29	356 ± 14	41.8 ± 23.1	(0.70 ± 0.39)×10^{-2}
0.3	**7**	1.27 ± 0.13	348 ± 36	361 ± 22	67.9 ± 24.5	(1.13 ± 0.41)×10^{-2}
1.8	**7**	0.76 ± 0.17	390 ± 38	395 ± 31	37.2 ± 20.5	(0.62 ± 0.34)×10^{-2}
	17	0.71 ± 0.15	401 ± 14	399 ± 16	56.7 ± 35.0	(0.95 ± 0.58)×10^{-2}
0	**7**	1.99 ± 0.24	314 ± 28	368 ± 34	fixed at 55	fixed at 0.92 × 10^{-2}
0.3	**7**	1.28 ± 0.19	361 ± 36	363 ± 21		
1.8	**7**	0.72 ± 0.11	402 ± 22	392 ± 33		
	17	0.73 ± 0.11	406 ± 26	401 ± 36		

*Gap between inversion and image planes

+f represents CBF, but with different units (ml/ml/s and ml/100 ml/min, resp.)

All data were fitted with Eq. [2] using two procedures: free fitting for all four unknowns CBV_a, Δ, δ_a, f and fitting only three unknowns CBV_a, Δ, δ_a assuming CBF = 55 ml/100 ml/min (f = 0.92×10^{-2} ml/ml/s, Table 1). The results were compared.

Mean values were calculated for each subject first and then averaged to get the inter-subject mean and standard deviation (SD). Only voxels with sufficient SNR were included (see Data Analysis).

Table 4

Gray matter CBV_a values in the brain.

Ref.	Species	Brain Region	Technique	CBV_a (ml/100 ml)
(12)	Human	whole brain	MRI (MEGESE)	0.74±0.20
(11)	Human	whole brain GM	MRI (QUASAR)	0.93±0.0
(17)	Human	whole brain GM	MRI (LL-ASL)	1.7±0.1
(40)	Human	anterior border zone	MRI (QUASAR)	0.88±0.07
		posterior border zone		1.19±0.11
		non-border zone GM		1.64±0.08
(64)	Human	whole brain GM	MRI (QUASAR)	0.67±0.16 *
This study	Human	whole brain GM	MRI (iVASO)	0.76±0.17
(15)	Human	whole brain	PET	1.1±0.4
(78)	Human	whole brain	PET	2.5±0.7+
(8)	Rat	whole brain	^{19}F NMR	0.9±0.2+
(79)	Rat	whole brain	^{19}F NMR	0.78+
(10,16)	Rat	cortex	MRI (MOTIVE and DW-ASL)	1.1±0.5
		caudate putamen		1.3±0.6
(80)	Rat	Somatosensory cortex	MRI (MOTIVE)	0.83±0.21

*This is from a reproducibility study including 28 cites across the world and a total of 284 healthy volunteers.

+In these studies, CBV_a values were reported as percentage of total CBV. They were therefore converted assuming total CBV of 5.5 ml/100 ml in human brain (4), and 3.1 ml/100 ml in rat brain (80).

Table 5

Arterial transit times in human *visual* cortex.

Ref.	Technique	Gap* (mm)	Δ (ms)	δ_a (ms)
(38)	Turbo-TILT	5	420±80	
(18)	LL-FAIR	6	423±33	573±62
(40)	QUASAR	30	540±20	
(37)	CASL	45	607±320	
This study	iVASO	7	390±38	395±31
This study	iVASO	17	401±14	399±16

*Gap between inversion and image planes